



# CHORUS

This is the accepted manuscript made available via CHORUS. The article has been published as:

## Enhanced superconductivity at the interface of W/Sr<sub>2</sub>RuO<sub>4</sub> point contacts

He Wang (□□), Weijian Lou (□□□), Jiawei Luo (□□□), Jian Wei (□□), Y. Liu, J. E. Ortmann, and  
Z. Q. Mao

Phys. Rev. B **91**, 184514 — Published 22 May 2015

DOI: [10.1103/PhysRevB.91.184514](https://doi.org/10.1103/PhysRevB.91.184514)

# Enhanced superconductivity at the interface of W/Sr<sub>2</sub>RuO<sub>4</sub> point contact

He Wang (王贺), Weijian Lou (娄伟坚), Jiawei Luo (骆佳伟), and Jian Wei (危健)\*  
*International Center for Quantum Materials, School of Physics, Peking University, Beijing 100871, China and Collaborative Innovation Center of Quantum Matter, Beijing, China*

Y. Liu

*Department of Physics and Materials Research Institute,  
The Pennsylvania State University, University Park, Pennsylvania 16802, USA and  
Department of Physics and Astronomy and Key Laboratory of  
Artificial Structures and Quantum Control (Ministry of Education),  
Shanghai Jiao Tong University, Shanghai 200240, China*

J.E. Ortmann and Z.Q. Mao

*Department of Physics, Tulane University, New Orleans, Louisiana 70118, USA*  
(Dated: May 4, 2015)

Differential resistance measurements are conducted for point contacts (PCs) between the Sr<sub>2</sub>RuO<sub>4</sub> (SRO) single crystal and the tungsten tip approaching along the *c* axis direction of the crystal. Since the contact is made at liquid helium temperature and tungsten tip is hard enough to penetrate through the surface layer, consistent superconducting features are observed. Firstly, with the tip pushed towards the crystal, the zero bias conductance peak (ZBCP) due to Andreev reflection at the normal-superconducting interface increases from 3% to more than 20%, much larger than previously reported, and extends to temperature higher than the bulk transition temperature. Reproducible ZBCP within 0.2 mV may also help determine the gap value of SRO, on which no consensus has been reached. Secondly, the logarithmic background can be fitted with the Altshuler-Aronov theory of electron-electron interaction for tunneling into quasi two dimensional electron system. Feasibility of such fitting confirms that spectroscopic information like density of states is probed, and electronic temperature retrieved from such fitting can be important to analyse the PC spectra. Third, at bias much higher than 0.2 mV there are conductance dips due to the critical current effect. These dips persist up to 6.2 K, possibly due to enhanced superconductivity under uniaxial pressure.

The layered perovskite ruthenate Sr<sub>2</sub>RuO<sub>4</sub> (SRO) has shown evidence for spin-triplet, odd-parity superconductivity (SC) which may be useful for topological quantum computation.<sup>1-3</sup> The possible chiral orbital order parameter for the two-dimensional SC is  $p_x \pm ip_y$  as suggested by the time-reversal symmetry breaking experiments.<sup>4,5</sup> Such chiral order is expected to generate edge currents, but the expected magnetic field due to edge currents has not been directly observed with local field imaging,<sup>6-8</sup> though there is indirect evidence of edge currents revealed by in-plane tunneling spectroscopy<sup>9,10</sup> and point contact spectroscopy (PCS),<sup>11,12</sup> both requiring assumptions to fit the conductance spectra and the fitting parameters including the gap value are not consistent with each other.

The surface properties of SRO is a critical factor for field imaging with scanning quantum interference devices, as well as for the tunneling and point contact spectroscopy. It is known that the SRO surface can undergo reconstruction and the intrinsic SC may not be probed,<sup>13,14</sup> and it may even show ferromagnetism (FM) due to lattice distortion.<sup>15</sup> Very careful *in situ* preparation of devices is required for making good tunnel junctions using microfabrication techniques.<sup>9</sup> Recently there is also theory proposal that surface disorder indeed can destroy the spontaneous currents.<sup>16</sup>

One way to overcome the surface layer problem is to use a hard tip for the point contact (PC) measurement.

If the tip is hard enough, it may penetrate through the surface dead layer and probe the SC underneath.<sup>17</sup> In fact, for this reason tungsten tip has been used for PCS of heavy fermion superconductors.<sup>18</sup> A consequence of using a hard tip is that the tip will exert some pressure on the surface which may affect the SC,<sup>19</sup> possibly due to local distortion of lattice.<sup>20,21</sup> It is known that for SRO a very low uniaxial pressure of 0.2 GPa along the *c* axis can enhance the superconducting transition temperature ( $T_c$ ) of pure SRO from 1.5 K up to 3.2 K,<sup>22,23</sup> and recently in-plane strain (0.23%) along  $\langle 100 \rangle$  direction is also shown to enhance  $T_c$  from 1.3 K up to 1.9 K.<sup>24</sup> The pressure in abovementioned measurements was applied to the whole crystal sample, while for PC the pressure is exerted locally on a small region of the sample. In the latter case it may be less affected by the inhomogeneity of the applied pressure and the sample is less tend to developing cracks, thus locally higher pressure may be reached although the absolute pressure is not known. Here we report greatly enhanced SC observed at the interface of the point contact junction between SRO single crystal and the tungsten tip approaching along the *c* axis direction.

SRO single crystals are grown by floating zone methods and are from two different batches, details of sample preparation can be found in previous reports.<sup>25</sup> The bulk  $T_c$  is about 1.5 K by standard resistance measurement. Sample S1 is from the first batch and is easier to cleave

and shows no Ru inclusions. Sample S2 is from the second batch, difficult to cleave, and contains a lot of Ru inclusions (for optical images of the surface and  $R(T)$  of the bulk samples, see Appendix C). Only on the freshly cleaved surface of S1 do we observe clear features of SC. Tungsten wire of 0.25 mm diameter is etched to form the tip. The silicon chip with the sample and thermometer glued on top is mounted on an attoCube nanopositioner stack. Since the tip and sample are both fixed to the copper housing, relative displacement between the tip and sample is suppressed, which ensures a stable contact and reproducible PC spectra. The housing is suspended with springs at the bottom of an insertable probe for a Leiden dilution fridge. With such customization, the sample position is not at the field center of the magnet, but the field value can be estimated with the tabled values from the magnet manufacturer. Differential resistance ( $dV/dI$ ) is measured with standard lock-in technique, and for easy comparison with theory, the reciprocal of  $dV/dI$  is plotted, which is close to  $dI/dV$  when the excitation is small.

At the same location, by pushing the tungsten tip towards the SRO surface (technically it is the SRO sample moving towards the tip), the PC resistance is reduced and the pressure is increased (see Appendix D for reproducibility and data acquired in other runs, see Appendix A for the model of PC resistance). The zero bias and zero field resistance ( $R_0$ ) is 9.3, 4.3, 3.2  $\Omega$  respectively, and the bias dependence of  $dI/dV$  is shown in Figs. 1(a), 1(c), and 1(e), at the nominal temperature 0.35 K. SC is clearly shown by the zero bias conductance peak (ZBCP), a dome like feature within  $\pm 0.2$  mV at zero applied field. With a 625 Oe magnetic field applied along the  $c$  axis ( $H_{\perp}$ ), SC is almost fully suppressed for the 9.3  $\Omega$  PC as shown by the conductance dip at zero bias. However, for the 4.3  $\Omega$  PC, there is still a small conductance dome at 625 Oe, suggesting that SC is not fully suppressed, *i.e.*, SC is enhanced with increased pressure.

Enhancement of SC is further confirmed by the temperature dependence of  $dI/dV$  at zero field as shown in Fig. 2(b) and Fig. 3(b), where  $T_c$  is increased from the bulk value of 1.5 K to about 2 K and 2.5 K for the 9.3  $\Omega$  and 4.3  $\Omega$  PC respectively. This enhancement of SC is consistent with previous susceptibility measurements on bulk SRO sample under uniaxial pressure, where the mechanism of  $T_c$  enhancement was ascribed to anisotropic lattice distortion,<sup>22,23,26</sup> similar to that found in the eutectic 3K phase.<sup>27,28</sup>

The magnetoresistance (MR) is shown in Figs. 1(b), 1(d), and 1(f) for the three PCs (for consistency with Figs. 1(a), 1(c), and 1(e), conductance is plotted, but MR is still used in description). The conductance starts to decrease quickly at around 400 Oe, and there is clearly a hysteresis with jumps which gets sharper and more pronounced for higher PC pressure (lower PC resistance). MR hysteresis is usually observed for ferromagnetic samples, and the observation of both features of SC and MR hysteresis can be linked to the coexistence of SC and ferromagnetism (FM), *e.g.*, for SC at the interface of ox-

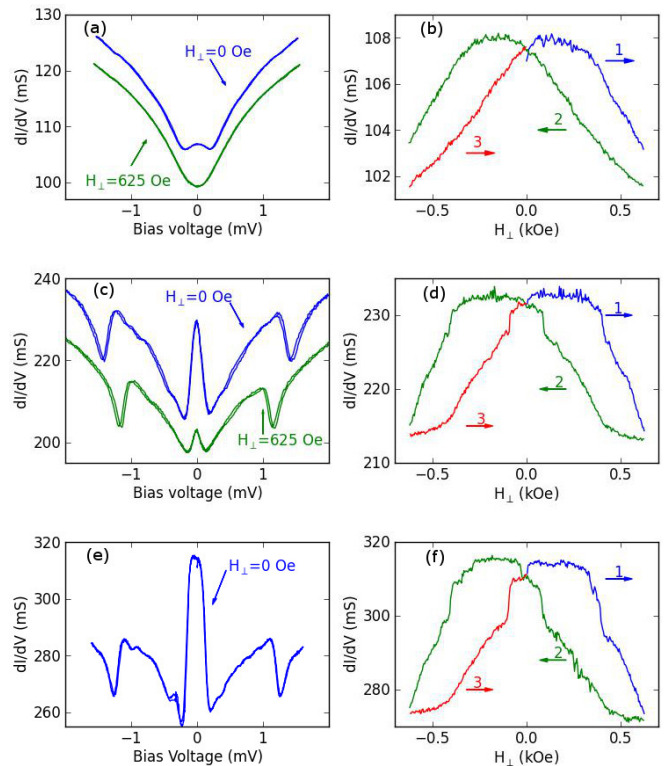


FIG. 1. (Color online) Bias dependence of  $dI/dV$  (a, c, e) and magnetoresistance (b, d, f) of three point contacts (PC) formed at the same location between the W tip and SRO single crystal S1 at 0.35 K. The resistance at zero bias and zero field ( $R_0$ ) is 9.3, 4.3, 3.2  $\Omega$  respectively. For clarity, in (a) and (c) the  $dI/dV$  curves at 625 Oe (Green) are shifted up by 2 and 10 ms respectively. Arrows in (b), (d), (f) show the sweeping direction of the magnetic field. The reproducibility of the measurements is demonstrated by the overlapping of  $dI/dV$  curves in (a), (c), (e) with bias ramping in both directions. The discontinuity around  $\pm 625$  Oe is related to the ramping speed of the field, and can be minimized when the field ramping speed is reduced, while the hysteresis is the same.

ides.<sup>29</sup> The question is whether the FM-like behaviour can be related to the time-reversal symmetry-breaking field.<sup>6-8</sup>

First the simple origin of vortex pinning needs to be considered. The field value above which  $dI/dV$  starts to decrease quickly is around 400 Oe, which is of the same order of magnitude as the upper critical field  $H_{c2}||c$  about 710 Oe for pure SRO crystal, but larger than the critical field  $H_{c1}||c$  about 70 Oe (by specific heat measurements).<sup>30</sup> Increase of resistance at around 400 Oe could be due to vortices entering the PC region and the SC fraction is reduced,<sup>21</sup> which would require a much enhanced  $H_{c1}$ . Although strongly enhanced  $H_{c1}$  by PC has not been reported, enhancement of  $H_{c2}$  due to pressure for a Nb tip was previously found.<sup>21</sup> For homogeneous vortex lattice the average distance between vortices is  $\sim \sqrt{\Phi_0/H}$ , about 0.3  $\mu\text{m}$  at 400 Oe. Thus to include

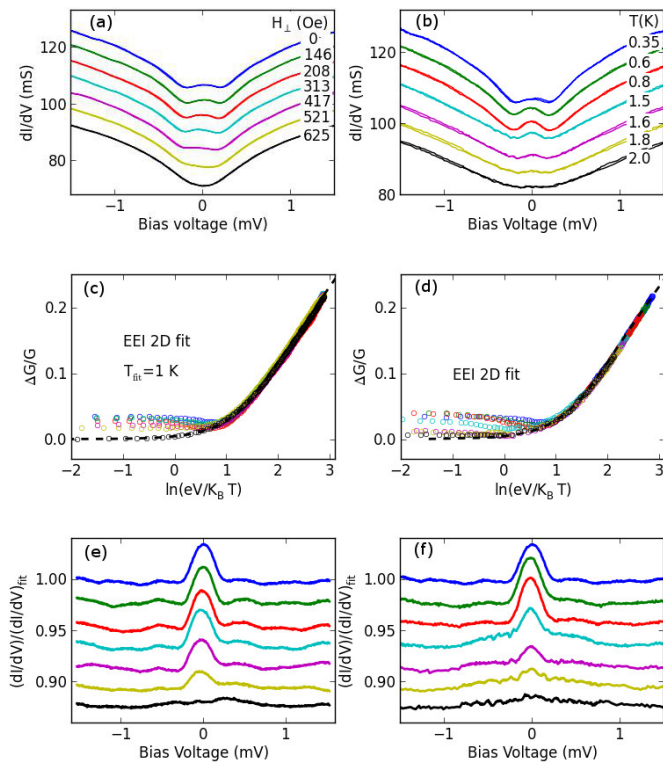


FIG. 2. (Color online) (a) Bias dependence of  $dI/dV$  for the  $9.3 \Omega$  point contact at  $0.35 \text{ K}$  with increasing  $H_{\perp}$  and (b) zero field  $dI/dV$  with increasing  $T$ . Curves are shifted for clarity except for the zero field  $0.35 \text{ K}$  curve. (c) Fitting with EEI theory in the 2D limit for data in (a) with fitting temperature  $T_{fit}=1.0 \text{ K}$ . (d) Fitting for data in (b) with  $T = 0.35 (1.0), 0.6 (1.1), 0.8 (1.24), 1.5 (1.65), 1.6 (1.85), 1.8 (1.95),$  and  $2.0 (2.2) \text{ K}$  from top to bottom ( $T_{fit}$  is indicated in the parentheses). After normalized by the EEI fits with corresponding  $T_{fit}$ , the curves are shown in (e) for different  $H_{\perp}$  and (f) for different  $T$ . Curves in (a), (b), (e), and (f) are shifted for clarity.

multiple vortices the diameter of the PC should be larger than  $0.3 \mu\text{m}$ . The estimation of the PC diameter with conventional model of the PC is tens of nanometer for PC resistance about  $10 \Omega$ , but if the model of distributed smaller PC junctions<sup>21,31</sup> is considered, then the area of the footprint can be much larger than the actual contact area within the footprint. Possibly related, a vortex droplet formed within a confined superconductor region can show discrete jumps of magnetization, which is associated with metastable vortex droplet and fission of vortices.<sup>32</sup> However, there is still some subtle difference, e.g., here for one ramping direction the MR jumps were found on both sides regarding to zero field, but in the droplet case the magnetization jumps only appear on one side. We also note that such large hysteresis was not observed previously in PC measurements, so although vortex pinning seems to be possible, it still needs to be confirmed.

Besides conventional pinning, intrinsic pinning due to chiral domain wall for SRO has been previously investi-

gated,<sup>33</sup> but it seems unlikely to reach  $400 \text{ Oe}$ . Note that hysteresis for threshold current was found by Kambara et al<sup>34</sup> in narrowed eutectic SRO bridges with Ru lamellae, where the assumption is that there is a domain wall (DW) between antiparallel domains with chiral supercurrent flowing in opposite directions. DW motion induced by DC current is proposed to be the origin of the hysteresis in the bias dependence of  $dI/dV$  measurements, but here we do not find hysteresis in the bias dependence of  $dI/dV$  measurements. Thus intrinsic pinning doesn't seem to be the origin.

Hysteretic vortex pinning has been reported for Superconductor-Ferromagnet nanocomposites (Nb matrix with Gd particles).<sup>35</sup> Surface FM on SRO was indeed predicted due to lattice distortion of surface reconstruction,<sup>15</sup> but was not experimentally confirmed. Among layered perovskite ruthenates in the series  $A_{n+1}Ru_nO_{3n+1}$ ,  $\text{SrRuO}_3$  is a ferromagnetic metal with  $T_c=160 \text{ K}$ , and  $\text{Sr}_3\text{Ru}_2\text{O}_7$  is at the boarder of FM and shows pressure-induced FM.<sup>36</sup> Thus it is not unexpected that FM could be induced for SRO, or there might be some eutectic phase<sup>25</sup> on the surface which leads to FM. Previously, experimental attempts to measure the magnetic susceptibility of bulk SRO with uniaxial pressure were unsuccessful, since above  $0.4 \text{ GPa}$  SRO sample tends to crush,<sup>37</sup> while no drastic change of the temperature dependence of susceptibility was observed. On the other hand, doping the Sr with Ca does show a ground state of *static* magnetic order due to rotation of  $\text{RuO}_6$  octahedra.<sup>38,39</sup> If the pressure under the tip is higher than  $0.4 \text{ GPa}$ <sup>17</sup> then the effect may be comparable with that by doping. In fact FM alone may lead to MR hysteresis in point contact measurements due to surface spin valve effect,<sup>40</sup> but here the hysteresis diminishes together with SC with increasing temperature (see Appendix E for the data), so there is still no clear evidence of surface FM.

Except for the MR hysteresis, both field and temperature dependences of  $dI/dV$  are similar to those found for in-plane Au/SRO tunneling junctions in Ref. [9], as shown in Fig. 2 and Fig. 3, for the  $9.3$  and  $4.3 \Omega$  PC respectively. We note that in Ref. [9] gap values  $0.7 \text{ mV}$ ,  $0.93 \text{ mV}$  (active), and  $0.28 \text{ mV}$  (passive) have been used to fit the in plane tunneling spectra, and the conductance enhancement of the dome like feature is less than 1% (we also observed similar PC spectra observed with a Au tip, see Appendix D). The dome like feature was fitted considering chiral *p*-wave symmetry in Ref. [9]. Since there are other possibilities for fitting the ZBCP, e.g., conventional *s*-wave superconductor near  $T_c$ , here we just focus on gap value instead of fitting the spectra with specific models. Besides Ref. [9], other gap values have been measured, e.g.,  $1.1 \text{ mV}$  from early Pt/SRO PC measurements,<sup>11,12</sup>  $0.38\text{-}0.5 \text{ mV}$  from early STM measurements,<sup>13</sup>  $0.28 \text{ mV}$  and  $0.35 \text{ mV}$  from recent STM measurements.<sup>14,41</sup> Here for W/SRO point contacts with different resistance and different pressure, and even in different locations and different runs, the  $0.2 \text{ mV}$  gap energy was observed consistently, and this gap value is comparable to that expected

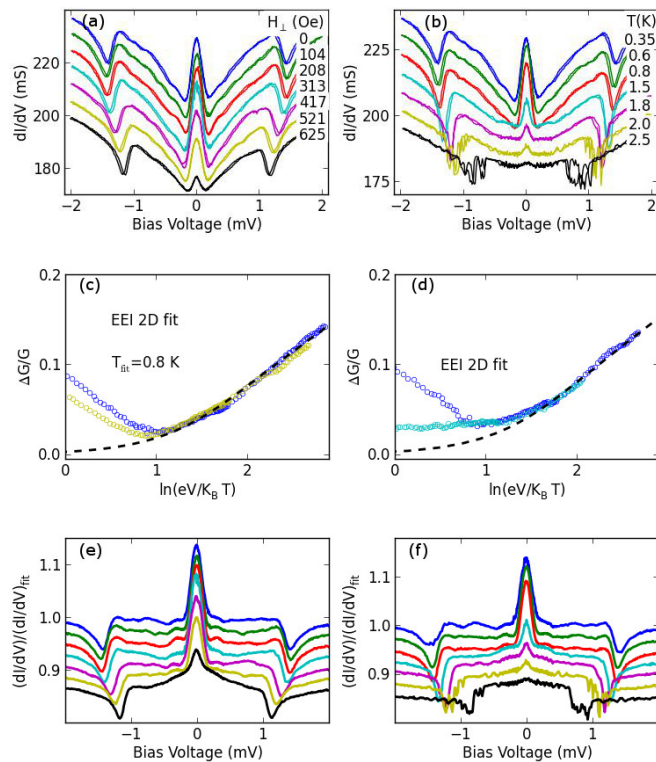


FIG. 3. (Color online) (a) Bias dependence of  $dI/dV$  for the  $4.3 \Omega$  point contact at  $0.35 \text{ K}$  and with increasing  $H_{\perp}$  and (b) zero field  $dI/dV$  with increasing  $T$ . Curves are shifted for clarity except for the zero field  $0.35 \text{ K}$  curve. (c) Fitting with EEI theory in the 2D limit for  $H_{\perp} = 0$  (blue) and  $625 \text{ Oe}$  (yellow) curves in (a) with  $T_{fit} = 0.8 \text{ K}$ , and (d) fitting for curves in (b) with  $T = 0.35$  ( $0.8$ ),  $1.5$  ( $1.5$ )  $\text{K}$  ( $T_{fit}$  is indicated in the parentheses). After normalized by the EEI fits with corresponding  $T_{fit}$ , the data curves are shown in (e) for different  $H_{\perp}$  and (f) for different  $T$ . Curves are shifted for clarity.

from  $T_c = 1.5 \text{ K}$  from mean field theory.

The broad background conductance dip in Fig. 1a for  $dI/dV$  at  $625 \text{ Oe}$  in is generally called zero-bias anomaly (ZBA), which is frequently observed in tunnel junctions<sup>9</sup> as well as PCs.<sup>12,42,43</sup> The possible origins for ZBA in PCs include “extrinsic” magnetic impurities, two-level systems, Kondo scattering due to spontaneous electron spin polarization etc, as well as “intrinsic” density of states (DOS) effect. Early PC measurements show that the DOS of chromium is reduced due to the spin density wave gap,<sup>44</sup> and recently for iron pnictides it is shown that DOS is enhanced due to strong electron correlations.<sup>31,45</sup> Since SC in SRO is very sensitive to impurities, and here ZBA apparently coexists with SC, so it is more likely due to “intrinsic” origin instead of impurities.

The background ZBA can be normalized when the bias dependence is replotted using  $\ln(eV/k_B T)$ . In Figs. 2(c) and 2(d), the normalized change of conductance shows a linear dependence for  $eV \gg k_B T$ , similar to what

was observed in tunneling measurements for disordered metal films,<sup>46</sup> and also for layered cuprates and manganites.<sup>47,48</sup> In the tunneling case, ZBA is attributed to the reduction of DOS due to electron-electron interaction (EEI), which can be also applied to PCS in the ballistic limit (see Appendix B for the justification of using tunneling theory for ballistic portion of the PC resistance). As proposed by Altshuler and Aronov<sup>49</sup> for low dimensional systems, EEI or more specifically the exchange interaction between electrons can cause quantum corrections to the conductivity and to the DOS, which depends on the dimensionality of the systems. For  $eV \gg k_B T$ , the DOS correction  $\sim \ln(eV/k_B T)$  in 2D. When the thermal smearing is taken account into the fitting and the full formula is used, we get good fits in the full bias range for the correction to conductance  $\Delta G/G$  as shown by the dashed lines in Figs. 2(c) and 2(d) (also in Figs. 1(a) and 1(b)).

We note that in order for all  $\Delta G/G$  curves to collapse onto the theoretical curve, an elevated temperature ( $T_{fit}$ ) needs to be assumed for data at lower temperatures, i.e.,  $eV/k_B T_{fit}$  is used instead of  $eV/k_B T_{bulk}$ , where  $T_{bulk}$  is the nominal temperature measured by the thermometer on the same silicon chip. This may indicate there is local heating in the small PC region, e.g., for PC in the thermal regime (see below and Appendix A for the model of PC resistance). Indeed at temperatures below  $1 \text{ K}$ , and particularly for mesoscopic samples, the electron temperature might be much higher than the bath temperature, in some cases due to inadequate filtering of the external microwave noise.<sup>50,51</sup> This elevated temperature may cause uncertainty to the fitting of ZBCP with  $p$ -wave symmetry, since even for  $s$ -wave SC, when  $T$  is close to  $T_c$  or the broadening parameter is large<sup>52,53</sup>, the frequently observed double-peak spectra may smear into a dome like feature for point contact junction with finite barrier (see e.g., Fig 5 in Ref. [19]). To check whether such dome like feature evolves to a double-peak like structure at lower temperatures, one needs to further cool down the PC, and an internal electron thermometer like  $T_{fit}$  from the EEI fitting is helpful.

The fitted curve can be considered as the normal state background and divided from the normalized conductance,<sup>9</sup> the resulted curves are shown in Figs. 2(e) and 2(f), with the dome like conductance enhancement well demonstrated. Another feature of the PC spectra in Figs. 2(e) and 2(f) is a small periodic “wiggling” outside  $\pm 0.2 \text{ mV}$ , which also diminishes with increasing field and temperature. Since the resistivity along  $c$  axis is about 1000 times larger than that in plane, the transport is presumably dominated by in plane transport. The “wiggling” may be due to in plane interference of quasiparticles for the S-PC (or S underneath PC)-S configuration, as suggested by the decreasing period with increasing PC conductance/diameter. Similar “wiggling” was also observed for the multiple band superconductor  $\text{MgB}_2$ ,<sup>17,19,54</sup> and scattering of quasiparticles between bands could be another origin for the oscillation. For

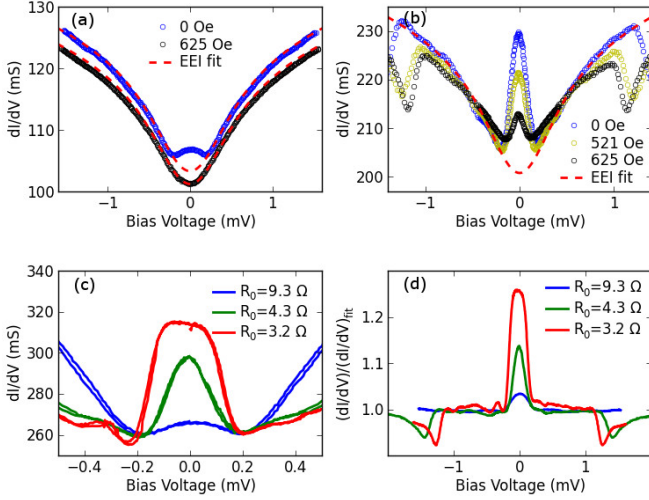


FIG. 4. (Color online) (a)  $dI/dV$  curves for the  $9.3 \Omega$  PC at 0 (blue), 625 Oe (black), and EEI fits (red dashed lines). (b)  $dI/dV$  curves for the  $4.3 \Omega$  PC at 0 (blue), 521 (yellow), 625 Oe (black), and the EEI fit for 0 Oe data. (c) Zoom-in of the zero bias resistance dip regime with curves shifted for clarity except for the  $3.2 \Omega$  curve. The curves are reproducible for both ramping directions of the bias. (d) Zero field conductance enhancement after normalized with the fitted EEI background. All at 0.35 K.

SRO, it was demonstrated<sup>9</sup> that multiple gap parameters could be involved in PC tunneling, which could be also related to the “wiggling”.

When the PC resistance is reduced from  $9.3 \Omega$  to  $4.3 \Omega$ , the ZBA background becomes less pronounced as shown in Figs. 3(c) and 3(d), while the conductance enhancement gets larger. This is better illustrated by the normalized enhancement (Fig. 4(d)), and by direct comparison of the zero field  $dI/dV$  (Fig. 4(c)). To explain these changes, conventional PC model (see Appendix A for details) can be introduced where the PC resistance is

$$R_{PC} = R_{Sh} + R_{Max}, \quad (1)$$

where  $R_{Sh}$  is the Sharvin resistance corresponding to the ballistic limit, and  $R_{Max}$  is the Maxwell resistance corresponding to the diffusive limit which is related to the bulk resistivity  $\rho$ . For the simplest metallic PC with the 1D ballistic transport assumption,  $R_{Sh}$  is energy independent as the energy dependence of velocity cancels that of the DOS. But when SC, EEI, or complicated (3D) Fermi surface are involved,<sup>31,44,45</sup> then the effective DOS may be probed by energy dependence of  $R_{Sh}$ , i.e., the PC spectra. Here for single crystal SRO the mean free path is large, and when the diameter of the PC is smaller than the inelastic scattering length, the PC is close to the ballistic limit. Note that for the practical situation where multiple smaller PC junctions are formed in parallel within the contact footprint, the effective area of PC is much smaller than that of the footprint.<sup>21,31</sup> In the conventional simple PC model  $R_{Sh} \propto (1/d)^2$  and

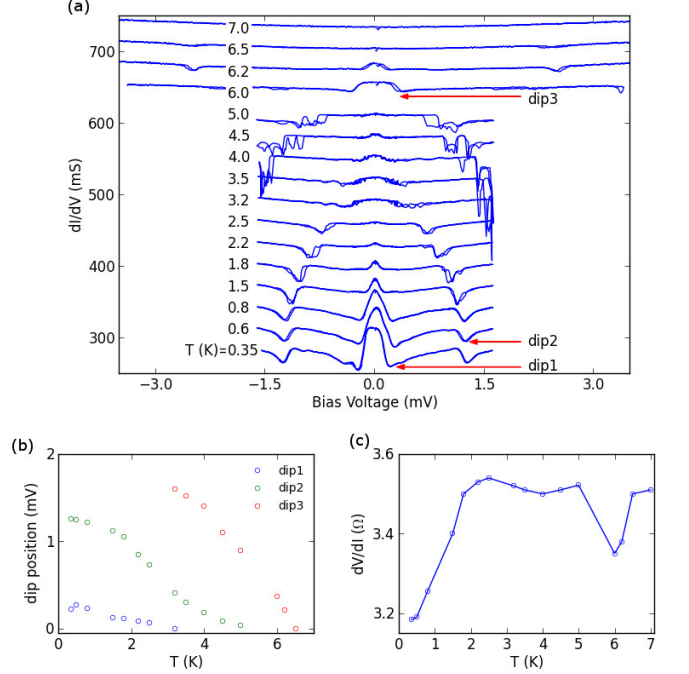


FIG. 5. (Color online) (a) For  $R_0=3.2 \Omega$  three SC transitions are shown by  $dI/dV$  dips at different temperatures. (b) The position of the  $dI/dV$  dips vs temperature. (c) Zero bias  $dV/dI$  vs. temperature. Both (b) and (c) are derived from (a).

$R_{Max} \propto (\rho/d)$ , where  $d$  is the diameter of PC, and  $\rho$  should be dominated by the in plane resistivity for SRO. The reduction of resistance from  $9.3 \Omega$  to  $4.3 \Omega$  suggests an increase of  $d$  by roughly  $\sqrt{9.3/4.3}=1.47$  times in the ballistic limit (twice increase of the area); or by 2.2 times in the thermal limit (quadruple increase of the area).

With the increase of contact area, the PC may show a larger critical current ( $I_C$ ) if the critical current density is constant and  $I_C$  is limited by the contact area. The additional  $dI/dV$  dips above 1 mV shown in Fig. 3 can be ascribed to the critical current effect<sup>55,56</sup>, where  $I_C$  of the  $R_{Max}$  in series with  $R_{Sh}$  is reached. And indeed the dips are more pronounced when the ratio of  $R_{Max}/R_{Sh}$  becomes larger when the total resistance  $R_{PC}$  gets smaller (see Appendix E for more measurement data). The  $R_{Max}$  is roughly  $0.1 \Omega$  as estimated by the resistance difference between the ZBA fit and the data curve above the dips. At 1.6 K the dip position is about 1.2 and 2.3 mV for the  $4.3 \Omega$  and  $9.3 \Omega$  PCs respectively, so the calculated  $I_C$  is around 0.28 and 0.25 mA respectively, inconsistent with the expected 2-4 times increase of  $I_C$  if it is proportional to the contact area  $\sim d^2$ . This finding suggests that  $I_C$  is determined by a fixed property, e.g., some SRO domain/surface regime under the PC, not just within the (effective) area of the PC itself. Thus, with increasing bias current, the  $R_{PC}$  shows a finite increase from  $R_{Sh}$  due to  $R_{Max}$ , as described in Eq.(1) and demonstrated

in Fig. 3.

When the PC resistance is further reduced to  $3.2 \Omega$  by pushing the tip to the SRO, even larger ZBCP is observed as shown in Fig. 1(e) and Fig. 4. After normalization by the background, the conductance enhancement at zero bias is about 3% for the  $9.3 \Omega$  PC, 14% for the  $4.3 \Omega$  PC, and 24% for the  $3.2 \Omega$  PC (Fig. 4(d)). The original  $dI/dV$  curves without normalization for the  $9.3$  and  $4.3 \Omega$  PCs are shown in Figs. 4(a) and 4(b), and the EEI fits can very well reproduce the conductance correction with an effective temperature  $T_{fit}$ . The EEI fit is no longer appropriate for lower  $R_{PC}$  when  $R_{Max}/R_{Sh}$  becomes larger, since above the critical current dip the increase of  $R_{Max}$  leads to a clear conductance drop, as shown in Fig. 4(d). Zoom-in the zero bias regime, the absolute amplitude of the ZBCP and of the “wiggling” are clearly shown in Fig. 4(c). We would like to emphasize again that for all three PCs in Fig. 4(c) the ZBCP evolves to ZBA background at around  $0.2$  mV, a gap value as expected from the weak-coupling theory.

The most striking feature is that the conductance dips persist to much higher temperatures than  $T_c$  of the bulk SRO, which is illustrated in Fig. 5. In Fig. 5(a), besides the first  $dI/dV$  dip at around  $0.2$  mV (this may not be a real dip but looks like one), there are two additional  $dI/dV$  dips, one persists up to about  $5$  K, while the other persists up to about  $6.2$  K. These two additional  $dI/dV$  dips are likely features related to SC, as the measured MR also shows hysteresis (see Appendix E for measurement data). The temperature dependence of the position of  $dI/dV$  dips is plotted in Fig. 5(b), and the zero bias  $dV/dI$  from the spectra in Fig. 5(a) is plotted in Fig. 5(c). There are clearly two resistance drops at around  $4$  and  $6$  K, and we note a similar but smaller resistance drop around  $4$  K was also observed in Ref. [9] for Au/SRO junctions. Since the bulk  $T_c \leq 1.5$  K for sample S1, and even for the 3-K phase  $T_c \sim 3$  K, thus here the greatly enhanced  $T_c$  should be only related to the W/SRO PC. Further investigation is required to clarify these probably new superconducting transitions.

In summary, an ultralow temperature point contact setup using nanopositioners was assembled and fresh contact interface can be made at liquid helium temperature to avoid surface reconstruction. Tungsten tip is used to penetrate the dead layer on surface. Differential resistance of W/SRO point contact junctions is measured and we find: 1) a dome-like shape of zero bias conductance enhancement within  $0.2$  mV, corresponding to a gap value comparable to that expected from mean field theory; 2) a broad conductance dip background coexisting with superconductivity, which is ascribed to density of states effect due to 2D electron-electron interaction, and the retrieved electronic temperature may be useful for further analyse of the point contact spectra; 3) SC-like features persisting up to  $6.2$  K, much higher than the bulk  $T_c$  of SRO, presumably due to the pressure exerted by the W tip.

We thank Hu JIN for contribution in the earlier stage

of this project, Liang LIU for various help with experiments and data analysis, Xin LU and Yi-feng YANG for helpful discussions on point contact measurements, and Fa WANG for discussions on correlated systems respectively. Work at Peking University is supported by National Basic Research Program of China (973 Program) through Grant No. 2011CBA00106 and No. 2012CB927400. The work at Tulane is supported by the DOE under grant DE-SC0012432.

## Appendix A: Model of point contact resistance

There are many reviews on point contact spectroscopy,<sup>57</sup> and particular on unconventional heavy fermion systems,<sup>58,59</sup> and recently on anisotropic and multiband superconductors.<sup>19,60</sup> Here we first introduce the basics of the PC resistance following Ref. 58, then add pertinent discussions regarding our system.

In the simplified theoretical model, PC is formed with an orifice with diameter  $d$  between two bulk metallic electrodes. Depending on the relative ratio between  $d$  and different mean free path  $l$ , PC can be categorized into three regimes: ballistic ( $d < l_{elastic}$ ), diffusive ( $l_{elastic} < d < l_{inelastic}$ ), and thermal ( $d > l_{inelastic}$ ). In the ballistic regime, the Fermi surface in the two electrodes has a difference of  $eV$ , similar to the tunneling junction case; while in the thermal regime, the Fermi surface evolves smoothly within the PC and there is a well defined equilibrium temperature profile.<sup>61</sup>

The current density in the orifice along its normal direction ( $z$ -axis) is

$$j_z = 2e \sum_k (v_k)_z f_k(E), \quad (A1)$$

where  $v_k$  is the electron velocity, and  $f_k(E)$  is the Fermi-Dirac distribution function. For a voltage biased ballistic PC, considering the energy difference  $eV$ ,

$$j_z = e \int_{E_F - eV/2}^{E_F + eV/2} dE \int \frac{d\Omega}{4\pi} v_z(E) f(E) N(E), \quad (A2)$$

where  $N(E)$  is the electronic DOS. In the simplified 1D case (similar to planar tunneling),  $v_z(E)$  is inversely proportional to  $N(E)$ , thus there is no non-linearity caused by energy dependence of DOS. The resulted Ohmic resistance is

$$R_{Sh} = \frac{16R_q}{(k_F d)^2} = \frac{16\rho l}{3\pi d^2}, \quad (A3)$$

where  $\rho$  is the bulk resistivity,  $l$  the elastic mean free path,  $R_q = h/2e^2 = 12.9$  k $\Omega$  the quantum resistance. With the assumption that the Drude picture holds,  $\rho l = p_F/n e^2$  is a constant for a particular metal, where Fermi momentum  $p_F$  and electronic density  $n$  were used in the original derivation. Thus, in the ballistic regime the diameter of the orifice  $d$  can be estimated using the zero

bias resistance  $R_0$ . To get a rough number, in the case of copper and other simple metals,  $d \sim 30/\sqrt{R_0(\Omega)}$  nm.

At finite bias, the electron can also be backscattered by phonons, magnons etc, at characteristic bias energy. So  $I$ - $V$  curve of the ballistic PC can be nonlinear and second derivative is often used to identify phonon and magnon spectra. For correlated materials with complex Fermi surface,  $v_z(E)$  is no longer inversely proportional to  $N(E)$ ,  $I$ - $V$  curve is nonlinear and  $R_{Sh}(E)$  may reflect the change of DOS.<sup>31,44,45</sup> More generally, other interactions like electron-electron interaction and superconductivity will also affect the DOS and be reflected in nonlinear  $I$ - $V$  curves or point contact spectroscopy.

For PC in the diffusive or thermal regime, electrons in the PC are (inelastically) scattered by impurities or defects, whose contribution to  $R_{PC}$  can be estimated from the bulk resistivity, and the orifice just provides a geometric limitation for integration. In the limit  $d \gg l_{inelastic}$ , the Maxwell resistance is

$$R_{Max} = \frac{\rho}{d}. \quad (A4)$$

As it depends on  $d^{-1}$  instead of  $d^{-2}$ , it dominates over  $R_{Sh}$  when  $d$  is large. And when inelastic scattering happens inside the PC region, the equilibrium temperature in the PC can be elevated following

$$T_{PC}^2 = T_{bath}^2 + \frac{V^2}{4L} \quad (A5)$$

where  $L$  is the Lorentz number. For a rough estimation, when  $T_{bath} \ll T_{PC}$ , assume a standard  $L = 2.45 \times 10^{-8} \text{ V}^2\text{K}^{-2}$ , then  $eV \sim 3.63k_B T_{PC}$ , or  $T_{PC}(\text{K}) \simeq 3.2V(\text{mV})$ . This suggests that in the thermal limit, similar feature can be found in the bias dependence of  $dI/dV(V)$  and in bath temperature dependence of  $dI/dV(T)$ . Here for SRO the gap energy is around 0.2 mV, in the thermal limit a rough estimation of  $T_{PC}$  at 0.2 mV is 0.64 K, which is still below  $T_C$  of SRO, so bias heating does not prevent observation of SC even in the thermal limit.

In the general situation, Wexler derived an interpolation formula,<sup>62</sup>

$$R_{PC}(T) \simeq \frac{16\rho l}{3\pi d^2} + \frac{\rho(T)}{d}. \quad (A6)$$

For a heterocontact between two different electrodes (1 and 2), the resistance has contribution from both sides. For geometrically symmetric PC with almost equal  $p_F$ ,

$$R_{PC}(T) \simeq \frac{16\rho l}{3\pi d^2} + \frac{\rho_1(T) + \rho_2(T)}{2d}. \quad (A7)$$

Since the resistivity of simple metal tip like tungsten is usually much smaller than that of the correlated electron systems (in normal state), we may just keep the resistivity term of the correlated systems being probed. The assumption of equal  $p_F$  is very rough, the difference between  $k_F = p_F/\hbar$  of tungsten and that of SRO is shown in Table I. Here  $k_F$  of tungsten is roughly estimated by

TABLE I. Summary of quasiparticle parameters of  $\text{Sr}_2\text{RuO}_4$  ( $\alpha, \beta, \gamma$ )<sup>2</sup> and Tungsten.

Fermi sheet	$\alpha$	$\beta$	$\gamma$	Tungsten
$k_F$ ( $\text{\AA}^{-1}$ )	0.304	0.622	0.753	1.55
$v_F$ ( $\text{ms}^{-1}$ )	$1.0 \times 10^5$	$1.0 \times 10^5$	$5.5 \times 10^4$	$1.8 \times 10^6$
$m^*$ ( $m_e$ )	3.3	7.0	16	1

assuming two valence electrons and a simple spherical Fermi surface.

In many cases it is found that although the footprint of the PC can be tens of microns, much larger than  $l$ , but still ballistic limit can be applied for fitting, which can be understood as that there are multiple smaller PC junctions randomly distributed across the contact region (the effective contact area is much smaller than the footprint).<sup>21,63,64</sup> Although conceptually this is different from the picture that there is an interface barrier which contributes to the PC resistance like a planar tunneling junction, but in both cases ballistic limit can be applied when  $R_{Sh}$  is much larger than  $R_{Max}$ . More generally, one can add a finite  $R_{Max}$  in series or parallel as a fitting parameter.

For a heterocontact between a normal metal and a superconductor, Blonder-Tinkham-Klapwijk (BTK) model<sup>65</sup> is widely used to explain the conductance enhancement within the gap energy. In the BTK model a tunnel barrier  $Z$  parameter is used to characterize the interface: for the clean interface, barrier parameter  $Z=0$ ; for the tunneling interface, barrier parameter  $Z_i=5$ , and there is a continuous transition from metallic to tunneling limit. Whether the Fermi velocity mismatch can be fully represented with an effective  $Z$  parameter is not yet clear.<sup>59</sup> Note that in BTK model inelastic scattering in the electrodes and the interface is not considered, even for finite  $Z$ , thus  $R_{Max}=0$ .

To take into account additional inelastic scattering at or near the interface, a finite  $R_{Max}$ , a normal resistor in series,<sup>56</sup> or a normal current in parallel<sup>21,64</sup> can be added to the tunneling term  $R_{Sh}$ . Thus even in the so-called thermal regime, it is possible to fit the PCS with the correct gap value with consideration of a combination of the BTK dominated  $R_{Sh}$  and some extra inelastic term  $R_{Max}$ .

When the SC has unconventional pairing symmetries, generalized BTK model is developed to fit the data by taking into account various parameters including order parameter symmetry, incidence angle, Fermi surface mismatch, life time broadening due to inter or intra band scattering etc. PCS for unconventional SC has been reviewed in Ref. 18, 19, 59, and 60. It is still not clear whether the order parameter symmetry can be verified strictly from the shape of the point contact Andreev reflection spectra. In this work we mainly report the temperature and field dependence of the PC spectra rather than quantitatively fit the data with the generalized BTK model.<sup>9,10</sup>

## Appendix B: Fitting with theory of electron-electron interaction

As discussed in Appendix A, most NS junction results can be well explained by the BTK model or generalized BTK models, where the tunneling barrier is characterized by the  $Z$  parameter, i.e., it can be thought as tunneling. In other words, the Sharvin resistance for ballistic transport can be understood as due to elastic tunneling of quantum tunneling channels with channel number equals  $(k_F d)^{-2}$  (see Eq. (A3)).

More specifically, the slight difference between tunneling and planar tunneling (ballistic point contact is approaching this limit) is whether the in-plane momentum is conserved. While STM measures the integrated density of states, point contact (or planner tunneling) measures an effective density of states with consideration of in plane momentum conservation.<sup>19,31</sup> This difference should be small for disordered films for which EEI is measured.

Correction to tunneling conductance by electron-electron interaction (EEI) due to reduction of density of states is quantitatively described by the Altshuler-Aronov (AA) theory,<sup>46,49</sup> in the 2D limit,

$$\frac{G(V, T) - G(0, T)}{G(0, T)} = \frac{e^2 R_{sq}}{8\pi^2 \hbar} \ln \frac{4\pi\delta}{\mathcal{D} R_{sq}} [\Phi_2(\frac{eV}{k_B T}) - \Phi_2(0)], \quad (\text{B1})$$

where  $R_{sq}$  is the resistance per square of the metal film,  $\delta$  the thickness of the insulating barrier,  $\mathcal{D}$  the diffusion constant, and  $\Phi_2$  a integral for 2D as defined in Ref. [46]. The integral is

$$\begin{aligned} \Phi_d(A) = & \int_{-\infty}^{\infty} dx \frac{\cosh(x+A) - 1}{\cosh(x/2)^2} \\ & \times \int_0^{\infty} dy \frac{\sinh y dy}{[\cosh y + \cosh(x+A)](1 + \cosh y)y^{2-d/2}}, \end{aligned} \quad (\text{B2})$$

where  $x = \epsilon/kT$  and  $A = eV/kT$ .

The prefactor before the bracket in Eq. (B1) can be lumped into one parameter  $S$  and it is the only fitting parameter. When  $eV \gg k_B T$  but still within the 2D limit, Eq. (B1) approaches  $S \ln \frac{eV}{k_B T}$  and  $S$  is just the slope shown in Fig. 2. Since  $R_{sq} = \rho/a$ ,  $a$  the thickness of the metal film, the resistivity  $\rho = (e^2 \nu \mathcal{D})^{-1}$ , the slope  $S \propto R_{sq} \ln(c\nu)$ , where  $c$  is a constant.

For the 3D limit,

$$\frac{G(V, T) - G(0, T)}{G(0, T)} = \frac{e^2 \rho}{8\sqrt{2}\pi^2 \hbar} (\frac{k_B T}{\hbar \mathcal{D}})^{1/2} [\Phi_3(\frac{eV}{k_B T}) - \Phi_3(0)], \quad (\text{B3})$$

which shows a linear dependence on  $\sqrt{eV/k_B T}$  when  $eV \gg k_B T$ .

In the main text Eq. (B1) is applied, and in Appendix D Eq. (B3) is used for PCs in other runs.

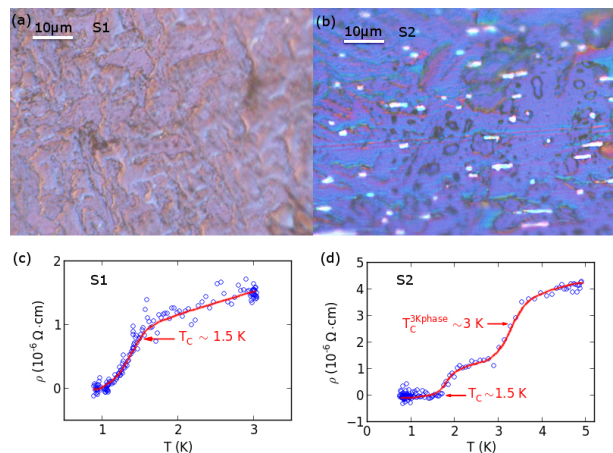


FIG. 6. (Color online) Comparison of polarized optical microscope images of sample S1 (a) and sample S2 (b). Ru inclusions are clearly seen in (b) for S2. Superconducting transition is shown for both samples by resistivity vs. temperature measurement in (c) and (d). The red lines are just guide to the eyes.

## Appendix C: Sample characterization

Optical images for SRO crystal samples S1 and S2 are shown in Fig. 6 for comparison. Dense Ru inclusions of width about  $1 \mu\text{m}$  and length a few  $\mu\text{m}$  are clearly seen in the micro image for S2, which is also harder to cleave than S1. This is consistent to the observation of Lichtenberg in Ref. 66 that SRO with Ru vacancies is much easier to cleave and the surface dead layer probably is also easier to pierce through. We note that although here the surface was polished by sandpaper to improve image quality, the Ru inclusions can easily be observed on the surface of S2 without any treatment.

In separate runs, conventional lock-in technique with room temperature transformer coupling was used to measure the temperature dependence of resistance for bulk samples. The lateral size of the samples is about 1 to 1.5 mm, the thickness about 0.5 mm, and the resistivity can be roughly estimated as shown in Fig. 6(c) and Fig. 6(d). Superconductivity of the SRO samples is verified and the transition temperature is around 1.5 K. We note that since the resistance is in  $\mu\Omega$  range large measurement current was applied which may cause some heating, so the temperature reading might not be accurate.

## Appendix D: Reproducibility

PC spectra for more than 10 locations were measured in several runs. In each run a few locations are tried to search for SC-like features. With increasing force the tip eventually became blunted and bent, and small cracks can also develop on the surface of the SRO. A set of PC spectra similar to that in the main text is shown in Fig. 7(a) for a W/SRO PC on S1 but obtained in another

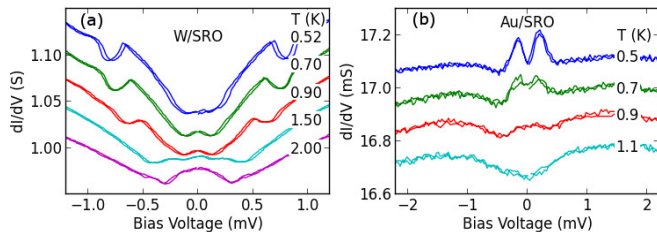


FIG. 7. (Color online) (a) Temperature dependence of the PC spectra for a W/SRO PC on S1 but obtained in another run, showing similar gap value and conductance dips as in the main text. The resistance is only about  $1 \Omega$ , so the heat dissipated around the PC should be larger. (b) Temperature dependence of the PC spectra for a Au/SRO PC on S1, a split peak within  $\pm 0.5$  mV is observed, similar to that in Ref. [9].

run. The gap value roughly around  $0.15$  mV is slightly smaller than  $0.2$  mV in the main text, possibly due to elevated local temperature, and the dips due to critical current effect at higher bias are again clearly shown.

Besides W tip, Au tip ( $0.5$  mm dia.) was also tried on S1 and one of the PC spectra is shown in Fig. 7(b). For the Au/SRO PC, gap value around  $0.5$  mV is observed, the conductance enhancement is only about  $1\%$ , and instead of the dome like conductance peak, a split peak is observed, both similar to those features reported for in-plane Au/SRO tunneling junctions in Ref. [9].

In Fig. 7(b) ZBA is less obvious, although for some other Au/SRO PCs we have observed much clearer ZBA and also conductance dips. For W/SRO PCs, ZBA is more frequently observed, which could be due to a smaller contact area (W tip doesn't deform like Au) and the thin barrier layer on the surface as observed in other PC measurements.<sup>64,67,68</sup> For those PC spectra showing clear ZBA, there are two typical types as shown in Fig. 8. One type is similar to that in Fig. 2 with a logarithmic dependence consistent with 2D EEI, and SC feature sometimes coexists with ZBA; the other type has a  $\sqrt{V}$  dependence which is consistent with 3D EEI, no clear SC feature is observed with this type of ZBA.

For the 2D EEI type, e.g., for a  $35 \Omega$  PC on S2 as shown in Fig. 8(c), the slope  $0.07$  is close to the slope  $0.11$  for S1 in Fig. 2, and  $0.08$  in Fig. 3, indicating similar 2D EEI is probed, though here  $T_{fit} = 2$  K is higher than the bath temperature about  $0.52$  K, which is probably the reason why SC is not clearly observed. On the other hand, for another  $13 \Omega$  PC on S2 as shown in Fig. 8(d), the fitted temperature is close to the bath temperature. And it is possible Ru inclusion is probed.

In early works, ZBA or conductance dip background was also observed for Pt/SRO PCs,<sup>12</sup> where with increasing field the ZBA becomes clearer and the origin is speculated to be related to some structural instabilities coupled to electronic and magnetic degrees of freedom. For in-plane Au/SRO tunneling junctions in Ref. [9], similar ZBA background was observed but only the normal state

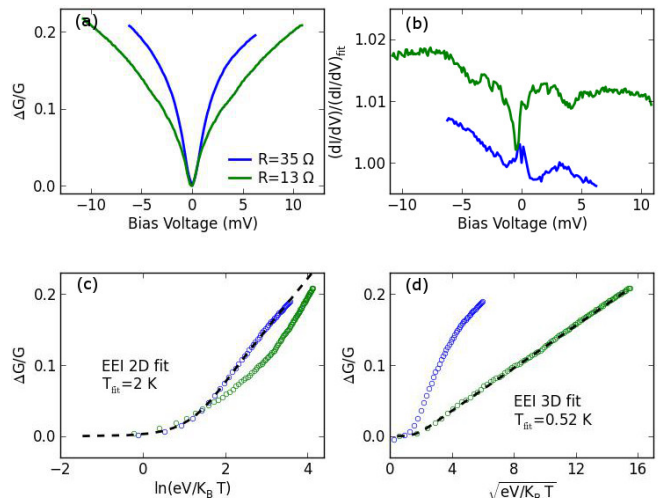


FIG. 8. (Color online) (a) Bias dependence of the normalized conductance for point contact on S2 with resistance  $35$  (blue) and  $13 \Omega$  (green) at  $T=0.52$  K, and (b) the conductance after normalized by the background EEI fits (the green symbols are shifted up for clarity). (c) EEI 2D fitting (black dash line) for the  $13 \Omega$  PC with  $T_{fit} = 2$  K, slope  $0.07$ . (d) EEI 3D fitting for the  $35 \Omega$  PC with  $T_{fit} = 0.52$  K, slope (3D) =  $0.015$ .

ZBA was used to normalize the PC spectra so the superconducting spectra were stressed, as has been done frequently for PCS. It is worth noting that in Au/Cu<sub>x</sub>Bi<sub>2</sub>Se<sub>3</sub> soft PCs, ZBA was also observed and ascribed to some pseudogap effect,<sup>68</sup> while later in another work such V-shape conductance background is considered due to non-ideal surface layer.<sup>64</sup> Our work may help clarify this issue and provide a more specific interpretation for ZBA or conductance dip background in PCS.

### Appendix E: Additional measurement data

For the  $3.4 \Omega$  point contact in the main text, magnetoresistance was also measured at two different temperatures as shown in Fig. 9(a). At  $4$  K, the hysteresis is still clear, and the total conductance change is close to that of the zero bias conductance enhancement due to SC as shown in Fig. 9(b). At  $8$  K, the hysteresis of MR is not clear, and the conductance decreases with increasing field, which is opposite to the trend in bias dependence of conductance. The above findings suggest that SC is still present at  $4$  K, but not at  $8$  K, and the MR hysteresis is closely related to SC.

To examine how much the critical current changes with point contact resistance, the normalized conductance for point contacts with different  $R_0$  is shown in Fig. 10(a) at fixed temperature  $1.8$  K. We note that between the measurements in Fig. 10(a), the tip was pushed against the crystal and point contact resistance decreased, also field and temperature ramping were conducted as shown

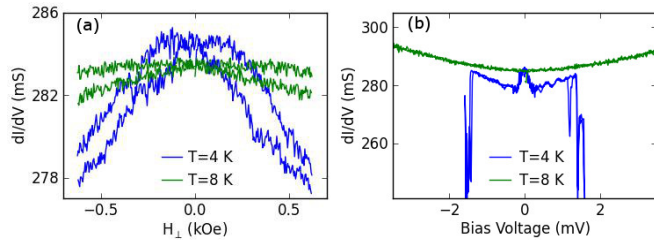


FIG. 9. (Color online) (a) Magnetoresistance at 4 K (blue) and 8 K (green) for the  $3.4 \Omega$  point contact. The hysteresis is clear at 4 K but not clear at 8 K since MR doesn't change much. (b) Bias dependence of the conductance for point contact at 4 K (blue) and 8 K (green) for the same contact, replotted with data in Fig. 5 for comparison with (a).

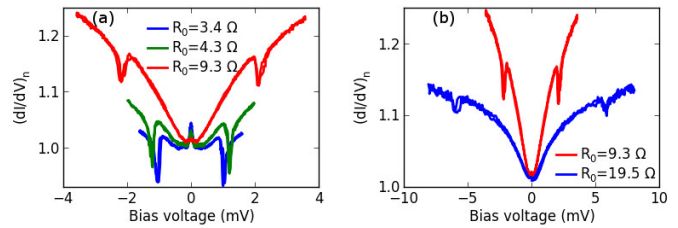


FIG. 10. (Color online) (a) Bias dependence of the normalized conductance for point contacts with different  $R_0$  at the same location, all at 1.8 K. The contact resistance decreases with increasing pressure. The critical current dips appear at bias voltage proportional to  $R_0$ . (b) At  $T = 1.9$  K, the position of the critical current dips for the  $19.5 \Omega$  PC is still proportional to  $R_0$ . The  $9.3 \Omega$  data from (a) are replotted here for comparison.

in the main text. The critical current can be roughly determined by the position of conductance dips (dip 2 in Fig. 5(a)), and is 0.29, 0.28, and 0.22 mA for 3.4, 4.3, and  $9.3 \Omega$  point contacts respectively, which is surprisingly close to each other, which has been discussed in the main text.

After the  $3.4 \Omega$  PC, the resistance was increased to  $19.5 \Omega$ . In Fig. 10(b), the conductance dips for  $9.3 \Omega$  and  $19.5 \Omega$  point contacts are compared. The critical current for the  $19.5 \Omega$  PC is about 0.3 mA at 1.9 K, close to that of the  $9.3 \Omega$  PC at 1.8 K. The relative size of the conductance dip becomes smaller for larger contact resistance, which can be understood since for larger  $R_{Sh}$ , the ratio of  $R_{Max}/(R_{Max} + R_{Sh})$  is smaller.<sup>55,56</sup>

\* weijian6791@pku.edu.cn

- <sup>1</sup> Y. Maeno, H. Hashimoto, K. Yoshida, S. Nishizaki, T. Fujita, J. G. Bednorz, and F. Lichtenberg, *Nature* **372**, 532 (1994).
- <sup>2</sup> A. P. Mackenzie and Y. Maeno, *Rev. Mod. Phys.* **75**, 657 (2003).
- <sup>3</sup> Y. Maeno, S. Kittaka, T. Nomura, S. Yonezawa, and K. Ishida, *Journal of the Physical Society of Japan* **81**, 011009 (2012), <http://journals.jps.jp/doi/pdf/10.1143/JPSJ.81.011009>.
- <sup>4</sup> G. M. Luke, Y. Fudamoto, K. M. Kojima, M. I. Larkin, J. Merrin, B. Nachumi, Y. J. Uemura, Y. Maeno, Z. Q. Mao, Y. Mori, H. Nakamura, and M. Sgrist, *Nature* **394**, 558 (1998), [cond-mat/9808159](http://dx.doi.org/10.1038/394558a).
- <sup>5</sup> J. Xia, Y. Maeno, P. T. Beyersdorf, M. M. Fejer, and A. Kapitulnik, *Phys. Rev. Lett.* **97**, 167002 (2006).
- <sup>6</sup> J. R. Kirtley, C. Kallin, C. W. Hicks, E.-A. Kim, Y. Liu, K. A. Moler, Y. Maeno, and K. D. Nelson, *Phys. Rev. B* **76**, 014526 (2007).
- <sup>7</sup> C. W. Hicks, J. R. Kirtley, T. M. Lippman, N. C. Koshnick, M. E. Huber, Y. Maeno, W. M. Yuhasz, M. B. Maple, and K. A. Moler, *Phys. Rev. B* **81**, 214501 (2010).
- <sup>8</sup> P. J. Curran, S. J. Bending, W. M. Desoky, A. S. Gibbs, S. L. Lee, and A. P. Mackenzie, *Phys. Rev. B* **89**, 144504

(2014).

- <sup>9</sup> S. Kashiwaya, H. Kashiwaya, H. Kambara, T. Furuta, H. Yaguchi, Y. Tanaka, and Y. Maeno, *Phys. Rev. Lett.* **107**, 077003 (2011).
- <sup>10</sup> S. Kashiwaya, H. Kashiwaya, K. Saitoh, Y. Mawatari, and Y. Tanaka, *Physica E: Low-dimensional Systems and Nanostructures* **55**, 25 (2014), topological Objects.
- <sup>11</sup> F. Laube, G. Goll, H. v. Löhneysen, M. Fogelström, and F. Lichtenberg, *Phys. Rev. Lett.* **84**, 1595 (2000).
- <sup>12</sup> G. Goll, *Physica B: Condensed Matter* **383**, 71 (2006), proceedings of the Third Hiroshima Workshop on Novel Functional Materials with Multinary Freedoms.
- <sup>13</sup> M. D. Upward, L. P. Kouwenhoven, A. F. Morpurgo, N. Kikugawa, Z. Q. Mao, and Y. Maeno, *Phys. Rev. B* **65**, 220512 (2002).
- <sup>14</sup> I. A. Firmo, S. Lederer, C. Lupien, A. P. Mackenzie, J. C. Davis, and S. A. Kivelson, *Phys. Rev. B* **88**, 134521 (2013).
- <sup>15</sup> R. Matzdorf, Z. Fang, Ismail, J. Zhang, T. Kimura, Y. Tokura, K. Terakura, and E. W. Plummer, *Science* **289**, 746 (2000).
- <sup>16</sup> S. Lederer, W. Huang, E. Taylor, S. Raghu, and C. Kallin, *Phys. Rev. B* **90**, 134521 (2014).
- <sup>17</sup> R. S. Gonnelli, A. Calzolari, D. Daghero, G. A. Umharino, V. A. Stepanov, P. Fino, G. Giunchi, S. Ceresara, and

- G. Ripamonti, *Journal of Physics and Chemistry of Solids* **63**, 2319 (2002), cond-mat/0107239.
- <sup>18</sup> K. Gloos, F. Anders, B. Buschinger, C. Geibel, K. Heuser, F. Jährling, J. Kim, R. Klemens, R. Müller-Reisener, C. Schank, and G. Stewart, *Journal of Low Temperature Physics* **105**, 37 (1996).
- <sup>19</sup> D. Daghero and R. S. Gonnelli, *Superconductor Science and Technology* **23**, 043001 (2010).
- <sup>20</sup> K. Gloos, F. Martin, C. Schank, C. Geibel, and F. Steglich, *Physica B: Condensed Matter* **206-207**, 279 (1995), proceedings of the International Conference on Strongly Correlated Electron Systems.
- <sup>21</sup> Y. Miyoshi, Y. Bugoslavsky, and L. F. Cohen, *Phys. Rev. B* **72**, 012502 (2005).
- <sup>22</sup> S. Kittaka, H. Taniguchi, S. Yonezawa, H. Yaguchi, and Y. Maeno, *Phys. Rev. B* **81**, 180510 (2010).
- <sup>23</sup> S. Kittaka, H. Yaguchi, and Y. Maeno, *Journal of the Physical Society of Japan* **78**, 103705 (2009), <http://journals.jps.jp/doi/pdf/10.1143/JPSJ.78.103705>.
- <sup>24</sup> C. W. Hicks, D. O. Brodsky, E. A. Yelland, A. S. Gibbs, J. A. N. Bruin, M. E. Barber, S. D. Edkins, K. Nishimura, S. Yonezawa, Y. Maeno, and A. P. Mackenzie, *Science* **344**, 283 (2014).
- <sup>25</sup> Z. Mao, Y. Maenoab, and H. Fukazawa, *Materials Research Bulletin* **35**, 1813 (2000).
- <sup>26</sup> H. Taniguchi, S. Kittaka, S. Yonezawa, H. Yaguchi, and Y. Maeno, *Journal of Physics: Conference Series* **391**, 012108 (2012).
- <sup>27</sup> Y. A. Ying, Y. Xin, B. W. Clouser, E. Hao, N. E. Staley, R. J. Myers, L. F. Allard, D. Fobes, T. Liu, Z. Q. Mao, and Y. Liu, *Phys. Rev. Lett.* **103**, 247004 (2009).
- <sup>28</sup> Y. A. Ying, N. E. Staley, Y. Xin, K. Sun, X. Cai, D. Fobes, T. J. Liu, Z. Q. Mao, and Y. Liu, *Nature Communications* **4**, 2596 (2013), 10.1038/ncomms3596.
- <sup>29</sup> D. A. Dikin, M. Mehta, C. W. Bark, C. M. Folkman, C. B. Eom, and V. Chandrasekhar, *Phys. Rev. Lett.* **107**, 056802 (2011).
- <sup>30</sup> K. Deguchi, Z. Q. Mao, and Y. Maeno, *Journal of the Physical Society of Japan* **73**, 1313 (2004).
- <sup>31</sup> W.-C. Lee, W. K. Park, H. Z. Arham, L. H. Greene, and P. Phillips, *Proceedings of the National Academy of Sciences* **112**, 651 (2015).
- <sup>32</sup> I. Lukyanchuk, V. M. Vinokur, A. Rydh, R. Xie, M. V. Milošević, U. Welp, M. Zach, Z. L. Xiao, G. W. Crabtree, S. J. Bending, F. M. Peeters, and W. K. Kwok, *Nature Physics* **11**, 21 (2015).
- <sup>33</sup> E. Dumont and A. C. Mota, *Phys. Rev. B* **65**, 144519 (2002).
- <sup>34</sup> H. Kambara, S. Kashiwaya, H. Yaguchi, Y. Asano, Y. Tanaka, and Y. Maeno, *Phys. Rev. Lett.* **101**, 267003 (2008).
- <sup>35</sup> A. Palau, H. Parvaneh, N. A. Stelmashenko, H. Wang, J. L. Macmanus-Driscoll, and M. G. Blamire, *Phys. Rev. Lett.* **98**, 117003 (2007).
- <sup>36</sup> S.-I. Ikeda, Y. Maeno, S. Nakatsuji, M. Kosaka, and Y. Uwatoko, *Phys. Rev. B* **62**, R6089 (2000).
- <sup>37</sup> S. I. Ikeda, S. Koiwai, Y. Yoshida, N. Shirakawa, S. Hara, M. Kosaka, and Y. Uwatoko, *Journal of Magnetism and Magnetic Materials* **272** (2004), 10.1016/j.jmmm.2003.12.1027.
- <sup>38</sup> J. P. Carlo, T. Goko, I. M. Gat-Malureanu, P. L. Russo, A. T. Savici, A. A. Aczel, G. J. MacDougall, J. A. Rodriguez, T. J. Williams, G. M. Luke, C. R. Wiebe, Y. Yoshida, S. Nakatsuji, Y. Maeno, T. Taniguchi, and Y. J. Uemura, *Nature Materials* **11**, 323 (2012).
- <sup>39</sup> J. E. Ortmann, J. Y. Liu, J. Hu, M. Zhu, J. Peng, M. Matsuda, X. Ke, and Z. Q. Mao, *Scientific Reports* **3**, 2950 (2013), 10.1038/srep02950.
- <sup>40</sup> I. K. Yanson, O. P. Balkashin, V. V. Fisun, Y. I. Yanson, and Y. G. Naidyuk, *Low Temperature Physics* **39**, 279 (2013).
- <sup>41</sup> H. Suderow, V. Crespo, I. Guillamon, S. Vieira, F. Servant, P. Lejay, J. P. Brison, and J. Flouquet, *New Journal of Physics* **11**, 093004 (2009).
- <sup>42</sup> K. Gloos, *Low Temperature Physics* **35**, 935 (2009).
- <sup>43</sup> K. Gloos and E. Tuuli, *Journal of Physics: Conference Series* **400**, 042011 (2012).
- <sup>44</sup> H. Meekes, *Phys. Rev. B* **38**, 5924 (1988).
- <sup>45</sup> H. Z. Arham, C. R. Hunt, W. K. Park, J. Gillett, S. D. Das, S. E. Sebastian, Z. J. Xu, J. S. Wen, Z. W. Lin, Q. Li, G. Gu, A. Thaler, S. Ran, S. L. Bud'ko, P. C. Canfield, D. Y. Chung, M. G. Kanatzidis, and L. H. Greene, *Phys. Rev. B* **85**, 214515 (2012).
- <sup>46</sup> M. E. Gershenson, V. N. Gubankov, and M. I. Faleš, *Sov. Phys. JETP* **63**, 1287 (1986).
- <sup>47</sup> A. A. Abrikosov, *Phys. Rev. B* **61**, 7770 (2000).
- <sup>48</sup> D. Mazur, K. E. Gray, J. F. Zasadzinski, L. Ozyuzer, I. S. Beloborodov, H. Zheng, and J. F. Mitchell, *Phys. Rev. B* **76**, 193102 (2007).
- <sup>49</sup> B. L. Altshuler and A. G. Aronov, *Sov. Phys. JETP* **50**, 968 (1979); B. L. Altshuler, A. G. Aronov, and P. A. Lee, *Phys. Rev. Lett.* **44**, 1288 (1980); B. L. Altshuler and A. G. Aronov, in *Electron-Electron Interactions in Disordered Systems*, Modern Problems in Condensed Matter Sciences, Vol. 10, edited by M. Pollak and A. L. Efros (North-Holland, Amsterdam, 1985) Chap. 1, pp. 1–154.
- <sup>50</sup> L. Liu, J. Niu, L. Xiang, J. Wei, D.-L. Li, J.-F. Feng, X.-F. Han, X.-G. Zhang, and J. M. D. Coey, *Phys. Rev. B* **90**, 195132 (2014).
- <sup>51</sup> J. Wei, S. Pereverzev, and M. E. Gershenson, *Phys. Rev. Lett.* **96**, 086801 (2006).
- <sup>52</sup> Y. Bugoslavsky, Y. Miyoshi, S. K. Clowes, W. R. Branford, M. Lake, I. Brown, A. D. Caplin, and L. F. Cohen, *Phys. Rev. B* **71**, 104523 (2005).
- <sup>53</sup> J. Wei, G. Sheet, and V. Chandrasekhar, *Appl. Phys. Lett.* **97**, 062507 (2010).
- <sup>54</sup> Y. Bugoslavsky, Y. Miyoshi, G. K. Perkins, A. D. Caplin, L. F. Cohen, A. V. Pogrebnnyakov, and X. X. Xi, *Phys. Rev. B* **69**, 132508 (2004).
- <sup>55</sup> L. Shan, H. J. Tao, H. Gao, Z. Z. Li, Z. A. Ren, G. C. Che, and H. H. Wen, *Phys. Rev. B* **68**, 144510 (2003).
- <sup>56</sup> G. Sheet, S. Mukhopadhyay, and P. Raychaudhuri, *Phys. Rev. B* **69**, 134507 (2004).
- <sup>57</sup> A. M. Duif, A. G. M. Jansen, and P. Wyder, *Journal of Physics: Condensed Matter* **1**, 3157 (1989).
- <sup>58</sup> Y. G. Naidyuk and I. K. Yanson, *Journal of Physics: Condensed Matter* **10**, 8905 (1998).
- <sup>59</sup> W. K. Park and L. H. Greene, *Journal of Physics: Condensed Matter* **21**, 103203 (2009).
- <sup>60</sup> D. Daghero, M. Tortello, P. Pecchio, V. A. Stepanov, and R. S. Gonnelli, *Low Temperature Physics* **39** (2013).
- <sup>61</sup> H. Pothier, S. Gueron, N. O. Birge, D. Esteve, and M. H. Devoret, *Phys. Rev. Lett.* **79**, 3490 (1997).
- <sup>62</sup> G. Wexler, *Proceedings of the Physical Society* **89**, 927 (1966).
- <sup>63</sup> Y. Bugoslavsky, Y. Miyoshi, G. K. Perkins, A. D. Caplin, L. F. Cohen, A. V. Pogrebnnyakov, and X. X. Xi, *Phys. Rev. B* **72**, 224506 (2005).

- <sup>64</sup> H. Peng, D. De, B. Lv, F. Wei, and C.-W. Chu, Phys. Rev. B **88**, 024515 (2013).
- <sup>65</sup> G. E. Blonder, M. Tinkham, and T. M. Klapwijk, Phys. Rev. B **25**, 4515 (1982).
- <sup>66</sup> F. Lichtenberg, Progress in Solid State Chemistry **30**, 103 (2002).
- <sup>67</sup> L. Shan, Y. Huang, H. Gao, Y. Wang, S. L. Li, P. C. Dai, F. Zhou, J. W. Xiong, W. X. Ti, and H. H. Wen, Phys. Rev. B **72**, 144506 (2005).
- <sup>68</sup> S. Sasaki, M. Kriener, K. Segawa, K. Yada, Y. Tanaka, M. Sato, and Y. Ando, Phys. Rev. Lett. **107**, 217001 (2011).